Conjugation-based genome engineering enables rapid prototyping and bioproduction in non-model bacteria

Michael S. Guzman[1,2*†], Cholpisit Kiattisewee[1,2,†], Jackson Comes[1,2+], Amanda M. Robert[1,2+], Ryan A.L. Cardiff[1,2], Margaret Cook[1,2], Allan Scott[3], Diego Alba Burbano[1,2], Stella Anastasakis[1,2], Sarah Grube[1,2], Kieran Heiberg[1], Brian Darst[1,2], Daniel Howell[1,2], Gara N. Dexter[4], Robert G. Egbert[3], Jesse G. Zalatan[1,2,5], Adam M. Guss[4], Joshua R. Elmore[3,*], Alexander S. Beliaev[3,*], James M. Carothers[1,2*]

1: Department of Chemical Engineering
University of Washington
Seattle, WA 98195
United States

2: UW Center for Synthetic Biology and Molecular Engineering & Sciences Institute
University of Washington
Seattle, WA 98195
United States

3: Biological Sciences Division, Pacific Northwest National Laboratory
Richland, WA 99354
United States

4: Biosciences Division, Oak Ridge National Laboratory
Oak Ridge, TN 37831
United States

5: Department of Chemistry
University of Washington
Seattle, WA 98195
United States

* Correspondence to:

Michael S. Guzman: msguzman@uw.edu
Joshua Elmore: joshua.elmore@pnnl.gov
Alex Beliaev: alex.beliaev@pnnl.gov
James M. Carothers: jcaroth@uw.edu

Abstract

Non-model bacteria offer unique metabolic capabilities for sustainable bioproduction, yet their limited genetic accessibility hinders systematic strain development. Here we present conjugation-based serine recombinase-assisted genome engineering (cSAGE), a broad-host-range platform that enables predictable, iterative genomic integration in transformation-resistant bacteria. cSAGE combines conjugative DNA delivery, standardized low-copy vectors, orthogonal recombinases, and modular genetic parts to support rapid pathway assembly and cross-host benchmarking. Using purple nonsulfur bacteria as a testbed, we integrate promoter engineering, multi-payload genome modification, and genome-scale metabolic modeling to empirically evaluate host-dependent pathway performance. Applying this workflow, we identify strain-specific differences in photosynthetic conversion of lignin-derived *p*-coumarate to the thermoplastic precursor *p*-vinylphenol. By enabling genome engineering and functional comparison across diverse bacteria using a single plasmid system, cSAGE provides a general framework for non-model strain prototyping and biotransformation discovery.

Introduction

Efficient microbial conversion of underutilized low-cost or waste-derived feedstocks into valuable products is central for a sustainable bioeconomy[1–4]. Across agricultural, chemical, and wastewater management sectors, large reservoirs of underutilized carbon exist in the form of volatile fatty acids[5,6], lignocellulosic residues[7], and industrial off-gases[8,9]. Harnessing these resources relies on leveraging the native metabolic capabilities of non-model bacteria and environmental isolates, together with engineered functions for efficient chemical and fuel production. Among these, purple nonsulfur bacteria (PNSB) represent a particularly versatile and underexploited group of microorganisms for bioproduction[10,11]. PNSB couple CO_2 fixation, photosynthesis, and carbon-efficient aromatic compound degradation within a single organism, allowing them to use low-energy infrared light to catabolize waste carbon feedstocks, including lignin-derived aromatics and syngas[12–18]. Despite their metabolic flexibility and the availability of curated genome-scale metabolic models predicting robust production capabilities[19–23], the use of PNSB for sustainable biomanufacturing remains limited by the lack of robust, stable, and host-agnostic tools[12,13,24]. Additionally, like many non-model organisms, the majority of PNSB species remain recalcitrant to transformation, creating a major bottleneck for strain engineering[25].

Over the past decade many advanced tools have been developed to address barriers in microbial genetics and engineering. However, these tools often have substantial limitations. For example, approaches such as CRISPR-Cas systems[26], transposon-based methods[27], or recombineering[28] are often limited by transformation efficiencies, host-range compatibility, and throughput of DNA integration[26,29]. Many of these methods require the use of replicating plasmids to achieve sufficient expression of the integration machinery, necessitating additional backbone-curing steps and restricting usage to hosts with compatible replication origins[26–28,30–32]. Moreover, replicating plasmids typically require prior screening of stable genetic parts for any given new organism[33]. As a result, genome integration strategies that perform well in a subset of species often fail to generalize across bacteria[34–38]. Beyond transformation efficiency and host-range, genome integration throughput presents a further fundamental limitation for non-model strain construction[39–41]. Widely used Tn7 transposon-based strategies typically only support a single integration event[30,42], while CRISPR-Cas systems require cloning of large, strain-specific homology-directed repair plasmids for each successive modification[31]. Although several of these systems are compatible with conjugative DNA delivery[30,42], they remain limited to single integrations and do not enable iterative integration of multiple genetic payloads within the same strain. This lack of scalable genome integration tools hinders the design and implementation of robust engineering cycles in non-model organisms.

Serine recombinase-based integration systems, by contrast, have recently emerged as powerful tools for genome engineering in non-model bacteria[43–47]. Serine-recombinase-assisted genome engineering (SAGE) enables site-specific, unidirectional integration of DNA into the host chromosome by catalyzing recombination between a plasmid-encoded, phage-derived attachment site (*attP*) and a corresponding bacterial chromosomal attachment site (*attB*)[48]. Once a poly-*attB* landing pad composed of multiple orthogonal *attB* sites is installed in the genome, SAGE supports efficient and stable integration of large or multi-gene pathways by allowing distinct recombinases to insert *attP*-flanked DNA cargos at specific *attB* sites. However, the deployment of SAGE has been limited by its reliance on electroporation for DNA delivery. Although electroporation is effective in many bacteria, the diversity and robustness of cell envelope composition often require optimization of electroporation conditions and competent cell preparation methods, which may ultimately prevent electroporation from working in some

species[39]. Thus, dependence upon electroporation as the sole DNA delivery method is a substantial barrier to utilizing SAGE across non-model bacteria.

Conjugation provides several advantages that make it a complementary method to electroporation for DNA delivery. First, conjugation is a highly conserved mechanism of horizontal gene transfer across the bacterial kingdom with functional range from laboratory *E. coli* strains to non-model microbes[49–51]. Second, conjugative DNA is initially transferred as single-stranded DNA and then replicated in the recipient cells, making it inherently more tolerant to restriction barriers than other delivery methods where double-standard DNA is directly exposed to host nucleases[52–54]. Accordingly, several recent broad-host-range genetic toolkits rely on conjugation as a robust and portable DNA delivery strategy across bacteria[55,56,57,30,42,58,59]. Conjugation has become the preferred method for introducing DNA into bacteria that are otherwise refractory to transformation, including PNSB, gut microbiota, marine and soil bacteria, and extremophiles[54,60–66].

Here we present conjugation-based SAGE (cSAGE), a broad-host-range genome engineering toolkit that combines the accuracy of serine recombinases with the efficiency of conjugative DNA transfer (Fig. 1). In cSAGE, all plasmids were redesigned in the Standard European Vector Architecture (SEVA) format[67,68] with an RK2/RP4 origin of transfer (*oriT*) for conjugative delivery[69] (Supplementary Fig. 1) and a *pir*-dependent R6K origin of replication that maintains plasmids at low copy in specialized donor strains and prevents replication in recipient hosts lacking the π replication protein (Pir)[70]. We paired this with a conjugation-compatible Tn7 strategy[42] for landing pad integration. A central feature of this design is that the same plasmid toolkit, built once, can be deployed across diverse bacteria without modification. We demonstrate this feature in a diverse panel of bacterial species, including several PNSB species, two *Pseudomonas* species and a *Rhodococcus jostii* (Table 1). Together, these results establish cSAGE as a foundation for predictive strain design and genome engineering across non-model Gram-negative and Gram-positive bacteria.

Results

Conjugation-based SAGE (cSAGE) enables efficient genomic integration in non-model bacteria

To expand the functionality of SAGE across diverse bacterial hosts, we introduced several key design modifications (Fig. 2). First, to enhance its portability, we redesigned all SAGE plasmids to be compatible with conjugation-based delivery by incorporating an origin of transfer (*oriT*). Second, to improve standardization and modularity, we transitioned the SAGE system into the Standard European Vector Architecture (SEVA) format, widely adopted for non-model bacterial hosts[67,68] (Supplementary Fig. 1). Lastly, to accommodate the potentially burdensome pathways in metabolic engineering applications, we migrated all SAGE vectors to low-copy, narrow-range R6K origins of replication that require the *pir* gene for replication[70]. This *pir*-dependent origin decreases plasmid copy number in cloning strains (e.g., *E. coli* pir$^+$), reducing metabolic burden[71,72], and ensures that plasmids do not replicate in most recipient strains following conjugation[70].

To evaluate cSAGE, we selected a diverse panel of PNSB, spanning the Alpha- and Beta-proteobacteria (Table 1)[73–76]. We first constructed base strains by integrating a poly-*attB* cassette into the genome (Fig. 2A). This cassette includes an array of 10 orthogonal *attB* sites (recombinase attachment sites), flanked by Rho-dependent transcriptional terminators to insulate downstream loci from transcriptional readthrough[44]. For *R. sphaeroides*[74], we used standard allelic exchange to integrate the poly-*attB* cassette into a type II restriction endonuclease site, *RshI*, responsible for restriction of foreign DNA. Knocking out *RshI* activity

was reported to improve transformation efficiency over the wild-type strain[77,78] (Fig. 2B). *R. palustris* CGA009, which was previously SAGE-enabled[44], was included here as a benchmark strain to validate cSAGE performance. For *R. palustris* P4[73], *R. rubrum*[75], and *R. gelatinosus*[76], a poly-*attB* cassette was integrated by an adapted Tn7 transposon-based strategy[42] (Fig. 2C). This strategy, which is compatible with Gram-negative bacteria, eliminates the need to construct host-specific allelic exchange vectors for landing pad integration, as a single, standardized plasmid can be used to SAGE-enable bacterial hosts.

We implemented a tri-parental mating strategy to deliver cSAGE components into recipient strains. In this approach, two *E. coli* donor strains–one carrying a payload plasmid with phage-derived attachment site (*attP*) for recombination and another donor carrying a serine recombinase expression plasmid for the corresponding *attP* site–are co-cultured with the recipient bacterium previously integrated with the poly-*attB* cassette (Fig. 2D). In the mixture of the three bacterial strains, the recipient strains, which receive two conjugative plasmids simultaneously, will express the serine recombinase for incorporation of the payload plasmid through a single crossover event. By using *E. coli* WM6026 as donor strains, with *pir*+ and Δ*dapA* genotypes for replicability of pR6K plasmids and auxotrophic selection, respectively, both cSAGE donor strains cease to grow after plating onto diaminopimelic acid (DAP)-deficient media. The only surviving cells are those with successful genome integration of the payload cassette, via selection of the antibiotic resistant marker, while non-replicative plasmids are lost in recipient strains.

We observed cSAGE to be functional across all five PNSB species tested, recovering transconjugants for nearly all of the recombinases tested using a standard reporter-based integration assay (Fig. 2E). To facilitate this comparison across recombinases and hosts within a consistent genetic context, we employed a reporter plasmid containing a poly-*attP* cassette, originally described by Elmore et al. (2023). This construct encodes a constitutively expressed mRFP reporter flanked by ten orthogonal *attP* sites corresponding to the poly-*attB* landing pad integrated in the recipient chromosome. When paired with a given recombinase expression plasmid, integration is directed specifically to the matching *attB* site, resulting in chromosomal insertion of the mRFP cassette detectable by fluorescence and confirmed by colony PCR. As a benchmark for cSAGE, we also measured conjugation efficiencies using a replicating plasmid (pBBR1), which is known to replicate across a broad range of Proteobacteria[79]. This control plasmid (pCK524) serves as an upper bound for conjugation efficiency, as plasmid transfer requires only a single conjugation event, in contrast to cSAGE, which requires delivery of two plasmids followed by site-specific recombination.

Both integration efficiency and accuracy influence the practical utility of a recombinase; therefore, we quantified both conjugation efficiency (frequency of transconjugant recovery) and integration accuracy (fraction of on-target integrations). While conjugation efficiency reflects DNA delivery and recombination activity, inaccurate or off-target integration can compromise strain stability and limit the utility of a recombinase for multi-cycle genome engineering. Bxb1, R4, and TG1 consistently demonstrated high efficiency across all species, at times comparable to pBBR1 (Fig. 2E). The remaining ϕC1, ϕBT1, RV and BL3 recombinases demonstrated variable efficiencies across species, with ϕC1 yielding detectable transconjugants only in *R. palustris* CGA009. Bxb1, TG1, R4, and RV were among the most precise recombinases tested across all five PNSB species. In contrast, other recombinases showed more variable accuracy.

Although no transconjugants were recovered in *R. gelatinosus* CBS using a pBBR1 replicating control plasmid, cSAGE integrations were successful in this host, underscoring the effectiveness of conjugation-based delivery of SAGE plasmids (Fig. 2E). To assess whether this portability extends beyond PNSB, we performed a limited evaluation in phylogenetically distinct bacteria, including *Pseudomonas putida* KT2440[80,81], *Pseudomonas sorgoleonovorans* SO8182,

and *Rhodococcus jostii* RHA1[83,84] with the three highest performing recombinases identified in PNSB (Bxb1, R4, and TG1) (Supplementary Fig. 2). Of note, electroporation of *P. sorgoleonovorans* was previously found to be highly inefficient, necessitating use of conjugation for gene deletion and DNA integration in previous work[82]. We observed detectable integrations across all three hosts, with variable conjugation efficiencies and integration accuracies. Although this dataset is not intended as a comprehensive benchmarking effort, these results demonstrate that cSAGE can function in bacteria spanning two phyla.

Iterative genome engineering workflows enabled by cSAGE

Iterative strain engineering in non-model bacteria involves repeated rounds of genomic integration to incrementally assemble complex or burdensome genetic programs, such as multi-gene metabolic pathways that cannot be introduced in a single step[39]. In practice, such workflows are limited by the repertoire of effective selectable markers[33,85] due to intrinsic resistance to antibiotics[24,86], and inconsistent performance of counterselection systems across species[85,87]. As a result, most existing approaches rely on sequential rounds of integration combined with intermediate marker or backbone removal to enable reuse of selectable markers, adding experimental steps and imposing additional host-specific requirements[37]. These limitations are particularly prevalent in non-model organisms such as PNSB where counterselection systems are often unavailable, unreliable, or require extensive characterization alongside selection markers[17,88–90]. Engineering strategies that enable rapid, iterative construction of multi-integrated strains without mandatory marker recycling remain scarce. This gap motivates the development of genome engineering workflows that decouple strain construction from marker recycling while still supporting optional marker excision when needed. To address this need, we developed two conjugation-compatible workflows: a multi-payload integration toolkit that enables sequential construction of marked strains without counterselection, and a ϕC31-based marker recycling strategy that supports removal of antibiotic resistance markers where compatible counterselection systems exist.

We hypothesized that multiple payloads could be integrated sequentially into cognate sites within the poly-*attB* landing pad without cross-recombination or interference. We designed payload plasmids containing distinct *attP* sites matched to orthogonal *attB* loci to enable independent recombinase-mediated integration events. We constructed three orthogonal serine recombinase systems–Bxb1, R4, and TG1–based on their strong performance and paired each with a unique antibiotic-resistance marker (Km^R, Sm^R, or Gm^R) for independent selection. As a proof of concept, we introduced orthogonal fluorescent reporters (mRFP, sfGFP, and mTagBFP2) as cargos into each of the three attachment sites. We performed sequential rounds of integrations in both *R. palustris* CGA009 and *R. sphaeroides*, selecting only for newly introduced antibiotic markers at each step and without intermediate excision of previously integrated backbones. Despite the introduction of repetitive pR6K backbone sequences from prior integrations, we observed stable fluorescence expression from all three reporters after each successive round of integration, with no detectable loss of signal or evidence of cassette dropout (Fig. 4B-C; Supplementary Fig. 4).

While the multi-payload integration strategy enables strain construction without backbone excision, the generation of antibiotic resistance-free strains remains essential for many downstream applications. In the SAGE system, ΦC31 integrase catalyzes excision of plasmid backbones flanked by *attP* and *attB* sites following payload integration, leaving behind only the desired cargo and a small recombination scar (attL) with minimal expected impact on host physiology[44]. However, ΦC31 integrase delivery in the original implementation relied on either a replicative mSF^{ts1} plasmid (a *Pseudomonas*-specific origin[91]) or a non-conjugative

pUC-derived plasmid[44], limiting applicability in PNSB where mSF^{ts1} does not replicate and electroporation is inefficient. To benchmark marker recycling and backbone excision in a fully conjugation-based workflow, we reimplemented the ϕC31 integrase helper plasmid in the conjugative pR6K vector. We constructed a poly-*attP* target plasmid that includes a constitutively expressed *mRFP* and a *sacB* gene for counterselection to evaluate this approach (Fig. 3A). We integrated this *sacB*-containing cargo into *R. palustris* CGA009 and *R. sphaeroides* via tri-parental conjugation using a Bxb1 integrase. Strains with the chromosomally integrated cargo then underwent diparental conjugation to deliver ϕC31-encoding pR6K plasmid. Following integration and counterselection on sucrose, we observed highly efficient marker curing in both species (Fig. 3B-C). In *R. palustris* CGA009, 16 of 16 colonies (100%) yielded the expected ~1.5 kb PCR product, indicating precise excision of the plasmid backbone (Fig. 3C). Similarly, in *R. sphaeroides*, 14 of 16 colonies (~88%) yielded the expected PCR product, whereas no detectable amplicon was observed for the remaining two colonies likely due to failed colony PCR reactions.

Together, these results demonstrate that cSAGE supports two complementary, fully conjugation-compatible workflows for iterative strain engineering in non-model bacteria. The multi-payload integration toolkit supports reliable, counterselection-free construction of multi-integrated strains, making it particularly well suited for workflows where rapid pathway assembly, testing, and comparison are prioritized. In parallel, ΦC31-mediated marker recycling provides an efficient route to generate antibiotic resistance-free strains when compatible counterselection systems are available. These capabilities establish a flexible engineering framework for strain construction that supports both rapid prototyping and deployment-ready strain construction.

Light-powered aromatic bioproduction in purple nonsulfur bacteria

PNSB represent one of the most metabolically versatile groups of microorganisms known, capable of thriving under anaerobic conditions while using infrared light energy and a broad range of inorganic and organic compounds as energy and carbon sources[11]. *R. palustris*, in particular, can oxidize diverse substrates, including CO_2, H_2, and organic acids, making them promising chassis for circular bioeconomy applications[12,13]. The ability of *R. palustris* to catabolize lignin-derived aromatics under anoxygenic conditions[92–95] further distinguishes these species as candidates for valorizing industrial waste streams such as lignocellulosic hydrolysates[17,94] and wastewater effluents[15,96]. However, this metabolic versatility is underpinned by complex regulatory networks that respond to light availability, O_2 tension, and nutrient status to control distinct carbon assimilation and redox balancing pathways[97]. Effective bioproduction in PNSB, therefore, requires not only understanding their metabolic potential but also genome-engineering tools that enable predictable control of heterologous pathway expression across species.

For well-studied PNSB such as *R. palustris* CGA009, genome-scale metabolic models (GEMs) provide a useful framework for predicting metabolic fluxes and evaluating production potential[98]. However, GEM construction is labor-intensive, requires extensive curation and experimental validation, and is often not readily transferrable even between closely related strains[99]. This limitation becomes particularly apparent when working with environmental isolates. For example, we recently sequenced and annotated the genome of the wastewater isolate *R. palustris* strain P4. Comparative genome analysis revealed numerous strain-level differences relative to CGA009, complicating *a priori* prediction of how native metabolism will interact with an engineered pathway (Supplementary Table 6 and 7). In this context, cSAGE provides an empirical approach to evaluate metabolically distinct but poorly characterized

environmental isolates for bioproduction. Rather than optimizing a pathway within a single host, our goal is to deploy identical genetic constructs across multiple hosts to reveal how host physiology shapes production outcomes.

To illustrate this capability, we focused on *R. palustris* strains as hosts for aromatic bioconversion. *R. palustris* species possess well-characterized pathways for uptake and catabolism of *p*-coumarate (*p*-CA) and related aromatics, including a conserved coumarate degradation operon (*CouABC* genes and associated transport systems[92,100]). Because substrate uptake and native catabolic capacity are prerequisites for conversion, *R. palustris* provides a relevant chassis for evaluating aromatic bioproduction. We therefore integrated BaPAD from *Bacillus atrophaeus*, which encodes a phenolic acid decarboxylase that converts *p*-CA to *p*-vinylphenol (*p*-VP)[101], a precursor for polymers[102], adhesives[103], and photolithography materials[104] (Fig. 5A). Because *R. palustris* strains differ in their genomic content (Supplementary Table 6 and 7), we hypothesized that host-specific physiology could strongly influence bioproduction outcomes even when the heterologous pathway remains identical (Supplementary Fig. 6).

Before integrating *BaPAD*, we used cSAGE to benchmark promoter activity across each host using a set of synthetic constitutive promoters characterized in *E. coli* and other Gram-negative bacteria[105,106] (Fig. 5B; Supplementary Fig. 5). Promoter characterization is crucial for programming heterologous gene expression. Even though the rank correlation of these synthetic promoters is generally conserved in previously characterized species[106], determining the precise expression levels is most reliable through experimental investigation. Using mRFP as a genetic reporter, we identified BBa_J23110 as a medium-strength promoter that performed consistently across species. Following genome integration of BBa_J23110::BaPAD using cSAGE, the engineered strains were cultivated photoheterotrophically in the presence of *p*-CA as the sole substrate (Fig. 5C, Supplementary Fig. 6).

The CGA009_BaPAD strain produced no detectable *p*-VP, suggesting complete catabolism of the substrate into biomass (Fig. 5C, Supplementary Fig. 7). Flux simulations using a GEM of CGA009_BaPAD[98] predicted no net flux towards *p*-VP production, instead routing carbon through native aromatic degradation pathways into central metabolic intermediates such as acetyl-CoA. In contrast, *R. palustris* strain P4_BaPAD whose capacity for aromatic catabolism had not been previously characterized, produced measurable amounts of *p*-VP, converting approximately 6% of the supplied *p*-CA into the desired product (Fig. 5C). The *p*-CA catabolic operon is completely conserved between CGA009 and P4 (Supplementary Fig. 6). Comparative analysis of KEGG orthologies predicted that P4 may encode additional functions related to phenylpropanoid metabolism, redox processes, and transport, suggesting that variation in redox balance, pathway regulation, or product export may underlie the observed divergence in *p*-vinylphenol production between strains (Supplementary Tables 6 and 7).

Together, these results demonstrate that host physiology plays a dominant role in determining pathway performance, even among closely related species. More broadly, this experiment illustrates how cSAGE enables direct evaluation of bioproduction pathways across hosts using empirical performance data. By enabling stable genome integration across hosts, cSAGE removes confounding factors associated with plasmid copy number and genetic instability. This capability provides a practical route to identify productive hosts early in the strain development pipeline, particularly for non-model organisms where predictive models are unavailable or insufficient.

Discussion

Advancing genome engineering in non-model bacteria requires overcoming one of the most common barriers in microbial synthetic biology: poor transformation efficiency[25]. Conventional domestication strategies scale poorly–each new host typically requires constructing bespoke allelic exchange vectors, compatible origins of replication, and genetic parts validated from scratch. cSAGE addresses this directly. By coupling conjugative DNA delivery with serine recombinase-mediated genomic integration and a narrow-range R6K vector backbone, the same pre-built donor system applies to new organisms with minimal development. Notably, cSAGE enabled genomic integration in *R. gelatinosus* despite the absence of detectable pBBR1 transfer, illustrating that the platform succeeds where standard broad-host-range tools fail. The multi-payload integration toolkit further decouples iterative strain construction from counterselection availability, enabling sequential integration of up to three orthogonal payloads without marker excision–a practical advantage in non-model bacteria where counterselection systems are often unreliable.

Our benchmarking of serine recombinases also raises broader questions about what drives efficiency and accuracy in bacterial systems. The variation we observe across recombinases (Fig. 2), even when expressed from identical promoters and delivered by conjugation, suggests that performance is primarily determined by intrinsic sequence preferences and host genomic context[107–112]. RV achieved 100% on-target integration across all five PNSB despite low overall conjugation efficiency (Fig. 2), suggesting that accuracy and efficiency reflect distinct mechanistic properties that can be independently optimized. Applying motif-scanning or pseudo-*attB* site prediction approaches to bacterial genomes could reveal the mechanistic basis for these differences and reduce the need for empirical screening when porting SAGE to new hosts.

The divergent *p*-VP production phenotypes observed between *R. palustris* CGA009 and P4 raise interesting questions about the basis of strain-level variation in pathway performance. Despite sharing a conserved *p*-CA catabolic operon (Supplementary Fig. 8), P4 produced measurable *p*-VP while CGA009 did not–aligning with GEM simulations that predicted complete *p*-CA flux through native degradation pathways in CGA009. The underlying basis for this divergence remains to be resolved, but comparative genomic analysis reveals that P4 encodes additional functions related to phenylpropanoid metabolism, redox processes, and transport relative to CGA009 (Supplementary Tables 6 and 7), any of which could contribute to the observed difference. Several non-mutually exclusive mechanisms could account for the divergence. Differences in *p*-CA import rate could alter the balance between BaPAD-mediated decarboxylation and native catabolic flux. For example, if CGA009 imports *p*-CA more efficiently, native pathway enzymes such as CouA (4-coumaroyl-CoA hydratase) may outcompete BaPAD for substrate. Alternatively, strain-level differences in regulatory control of the coumarate degradation (*cou*) operon could affect how quickly catabolic flux is activated in response to *p*-CA. Finally, *p*-VP export capacity may differ between strains. Given the acidity of *p*-VP and its potential for intracellular toxicity, efficient export would be expected to drive net product accumulation. We quantified only extracellular *p*-VP and did not directly measure intracellular pools. Distinguishing among these possibilities will require targeted experiments, including flux measurements, transporter knockouts, and *in vitro* enzyme assays.

By combining broad-host-range genome engineering with photosynthetic chassis, cSAGE extends the reach of the circular bioeconomy into organisms capable of valorizing underutilized carbon streams. The ability of PNSB to integrate CO_2 fixation, aromatic catabolism, and phototrophic growth positions them as uniquely powerful platforms for carbon-neutral bioproduction from lignin-derived aromatics, organic acids, and syngas. The

multi-payload integration and promoter characterization enabled here lay the groundwork for predictive strain design and for coupling genome engineering with metabolic and systems-level models[20,98]. Beyond PNSB, cSAGE also extends to taxonomically diverse organisms including Gram-positive *R. jostii* RHA1 and Gram-negative *P. putida* KT2440 and *P. sorgoleonovorans* SO81 (Supplementary Fig. 2), relevant to bioremediation[84], bioproduction[81], and agriculture[82], confirming that the platform is not confined to any single phylogenetic group. Broadly, cSAGE serves as a platform technology for expanding genetic accessibility across non-model bacteria, supporting the development of broad-host-range CRISPR-based regulation[113,114], synthetic pathway construction[115], and genetic code expansion[116].

Methods

Plasmid and strain construction

Plasmids used in this study are listed in Supplementary Table 2. All cSAGE plasmids were assembled in the Standard European Vector Architecture (SEVA) format. Plasmids were constructed either using In-Fusion, unless otherwise noted, and verified by whole-plasmid Nanopore sequencing. A complete list of plasmids, assembly primers, and notes can be found in Supplementary Table 5. Base strains carrying poly-*attB* landing pads were generated for each PNSB host to enable site-specific integration. *R. sphaeroides* landing pads were integrated by two-step allelic exchange using pK18mobSacB-derived vectors, whereas *R. palustris* P4, *R. rubrum*, and *R. gelatinosus* landing pads were delivered by a Tn7 transposon-based system we adapted for this study, where a Tn7 delivery vector carrying the poly-*attB* cassette and flanking FRT sites allows for subsequent excision of the antibiotic resistance marker. We used PCR to verify correct cassette insertion into each organism. Reporter and pathway integration strains were generated by tri-parental conjugation using *E. coli* WM6026[117] donors carrying the integrase expression plasmid and the cognate *attP* payload plasmid. Single colonies were screened for correct integration by colony PCR and reporter fluorescence, and confirmed integrants were archived for subsequent engineering steps. For sequential integration experiments, orthogonal serine integrases (Bxb1, TG1, and R4) were paired with distinct antibiotic resistance markers and reporters (sfGFP, mKate2, and mTagBFP2) to enable iterative selection without marker curing, as described in the section “Sequential integration of multiple payloads”. Marker recycling was performed using ΦC31 integrase-mediated excision and *sacB* counterselection, as described in the section “Marker recycling via ΦC31 integrase and *sacB* counterselection”.

Serine recombinase screening assays

To assess integrase performance across hosts, we used a standard tri-parental conjugation protocol to deliver both the non-replicating poly-*attP* target plasmid and the corresponding non-replicating integrase expression plasmid into recipient strains (Supplementary Table 2). All conjugations were carried out using the *E. coli* donor strain WM6026, which carries the *pir* genes necessary for R6K replication and is auxotrophic for diaminopimelic acid (DAP) to allow for counterselection post-mating. Donor WM6026 cells were grown overnight in LB with 0.1 mM DAP and appropriate antibiotics. Separately, PNSB recipients were cultured in rich medium (e.g., 3xYPS-MOPS for *R. palustris*, LB for *R. sphaeroides*) for 2–5 days until mid- to late-log phase. For tri-parental conjugations, WM6026 carrying the integrase plasmid and WM6026 carrying the poly-*attP* target plasmid were each washed and mixed with the recipient strain at equal optical densities (OD_{600} = 1.0) in a 1:1:1 ratio. The cell mixtures were centrifuged, resuspended in ~50 µL of fresh media, and spotted onto non-selective agar plates supplemented with 0.1 mM DAP and incubated overnight (~16 h) to allow for conjugative DNA transfer and recombination. After overnight incubation at 30°C, conjugation mixtures were harvested, washed three times in fresh medium to remove residual DAP, and serially diluted for plating onto selective agar (lacking DAP) containing the appropriate antibiotic for selection of a single-*attP* or poly-*attP* target plasmid. Control recipient-only plates were used to quantify conjugation efficiency as transconjugants per viable recipient. Colonies were counted after 3–5 days of incubation at 30°C. Integration accuracy was assessed by colony PCR using a primer flanking the intended *attB* site and a single primer internal to the integrated target plasmid (Supplementary Table 4). In *R. palustris* CGA009 and P4, *R. rubrum*, and *R. gelatinosus*, kanamycin selection (poly-*attP* plasmid pSA29) was used to quantify conjugation efficiency following delivery of the payload and recombinase plasmids. However, in *R. sphaeroides*, kanamycin selection proved unreliable, likely due to antibiotic marker incompatibility, so we

substituted spectinomycin (poly-*attP* plasmid pAR38) as the selectable marker unless otherwise indicated (Supplementary Fig. 3). Conjugation efficiencies were determined as the number of colonies on selective media (transconjugants) per number of viable recipient cells. This allowed us to directly compare integration efficiency across strains and recombinases.

Reporter fluorescence quantification

Single colonies were inoculated in a 2 ml 96-DWP containing rich broth media with antibiotic selection (500 µL media). Plates were incubated at 30°C on a plate shaker for 24-48 h to enable sufficient outgrowth and fluorescent reporter expression. Optical density (OD_{660}) and flourescence were measured on a BioTek Synergy H1 plate reader and compared to WT controls to ascertain RFU/OD_{660}. The following plate reader settings were used, unless otherwise noted: sfGFP: 485nm/528nm, mTagBFP2: 400nm/455nm, and mRFP 540nm/600nm.

Promoter activity assays

To benchmark promoter activity in *R. palustris* CGA009 and *R. sphaeroides*, Anderson series (https://parts.igem.org/) promoters were cloned upstream of an mRFP reporter and integrated into the genome at the SAGE landing pad (Supplementary Tables 2 and 3). Strains were cultivated under routine aerobic cultivation conditions at 30°C, and fluorescence was measured (Ex/Em: 545nm/591nm) and calculated as described above.

Marker recycling via ϕC31 integrase and sacB counterselection

To enable antibiotic marker recycling following integration, we adapted a marker curing strategy using ϕC31 integrase-mediated excision and *sacB*-based counterselection (Elmore et al. 2023). PNSB strains containing a genomically integrated poly-*attP* target plasmid (pMG97 or pJC009) were used as recipients for the ϕC31 plasmid (pSG010). WM6026 donor strains harboring the non-replicating ϕC31 integrase expression plasmid were prepared as described above and conjugated into these strains using di-parental mating. After mating, cells were plated onto agar containing sucrose (concentrations used for each strain are noted in Supplementary Table 4), excluding DAP, to select for marker loss and counterselect *E. coli*. Purple colonies appearing after 3–5 days of incubation at 30°C were screened by colony PCR using primers flanking the Bxb1 *attB* site (Supplementary Table 4). Successful marker curing was indicated by the loss of the antibiotic marker and plasmid backbone, while retention of the payload was verified by *mRFP* fluorescence.

Sequential integration of multiple payloads

To demonstrate multi-payload genome engineering using cSAGE, we constructed a three-plasmid toolkit in which each plasmid encodes a different fluorescent reporter (sfGFP, mTagBFP2, or mRFP), a unique integrase attachment site (Bxb1, R4, or TG1), and an orthogonal antibiotic resistance marker (Km^R, Sm^R, or Gm^R). Integration was performed sequentially in *R. palustris* CGA009 and *R. sphaeroides* using tri-parental conjugation as described above, starting first with mTagBFP2 (pJC001), then mRFP (pMG083 for CGA009 or pJC008 for *R. sphaeroides*), and lastly, sfGFP (pBD0132). After each integration round, transconjugants were screened for reporter expression and validated by colony PCR to confirm integration at each intended *attB* site (Supplementary Table 4). Confirmed single-copy integrants were subcultured and used as recipients for the subsequent integration. Each round of integration was performed using only the antibiotic marker relevant to the newly introduced plasmid, with no selection for previously integrated markers. Fluorescence was quantified for each strain to evaluate reporter expression and confirm stable maintenance of all three integrated payloads.

Genomic integration of BaPAD

p-VP producing strains were generated by tri-parental conjugation of pRC442 (J23110::BaPAD) and pCK1205 (Bxb1 helper plasmid) with either *R. palustris* CGA009 (JE4632), *R. palustris* P4 (sMG127) or *R. sphaeroides* 2.4.1 (AVS4) (Supplementary Table 1). pRC442 contains a codon-optimized phenolic acid decarboxylase gene from *Bacillus atrophaeus* (BaPAD), the BxbI *attP* site, and a kanamycin selection marker. Successful integrants were screened as described above.

Bioproduction of p-vinylphenol

Metabolites were quantified by preparing a standard curve in Sistrom's media and fitting it to a linear equation. Media containing *p*-coumarate (*p*-CA) was prepared as previously described[118]. As a result of *p*-CA insolubility, sonication followed by filtration was used to make 10 mM *p*-CA in Sistrom's minimal media. *R. palustris* strains were fed exclusively *p*-CA. Subsequent bioproduction experiments were inoculated from a starting anaerobic culture. Cultures were incubated at 30°C with infrared light until reaching stationary phase (7 days), at which point they were sampled periodically. For quantitative analysis, 1 mL of cell cultures were extracted using a 1 mL syringe and centrifuged for 5 min at 20,000xg. Supernatants were loaded into 0.2 µm, 10 kDa PES polypropylene filter 96-well plates (Analytical, cat. no. 964014) and centrifuged for 20 min at 1,500xg. *p*-vinylphenol (*p*-VP) and *p*-CA were quantified using High-Performance Liquid Chromatography (HPLC). Filtered supernatants were collected in HPLC vials with piercable caps. Samples were analyzed by injecting 50 µL into an Agilent HPLC system equipped with a diode array detector set at 254 nm and 310 nm and separated using a ZORBAX RX-C18 reverse-phase column (4.6 nm x 150 nm, 5 µm particle size; Agilent Technologies). The mobile phases were (A) acetonitrile plus 0.1% Trifluoroacetic acid (TFA), and (B) water plus 0.1% TFA. The flow was held at 1.000 mL/min. The mobile phase gradient follows: hold at 10% solvent A from 0.0 to 2.0 min, 10% to 50% solvent A from 2.0 to 12.0 min, hold at 50% solvent A from 12.0 to 14.0 min, 50% to 10% solvent A from 14.0 to 14.5 min, hold at 10% solvent A from 14.5 to 20.0 min. The retention times for the detected compounds were: 11.5 min (*p*-VP) and 7.1 min (*p*-CA). *p*-CA and *p*-VP concentrations were determined according to a standard curve of known concentrations (Supplementary Fig. 7).

Optical density measurements

Optical density (OD_{660}) of bacterial cultures in Hungate tubes was measured using a custom-built, non-invasive photometer adapted from the TubeOD design[119]. The device consists of a 3D-printed tube holder with an LED (596 nm) and a photosensor positioned on opposite sides of the culture tube to measure transmitted light (Supplementary Fig. 9). Light intensity was recorded as an analog voltage inversely proportional to cell density and logged using a LabJack U3-HV. Species-specific calibration curves were generated relative to a benchtop spectrophotometer and used to convert voltage to OD_{660} values. Python scripts are located on the GitHub repository https://github.com/Kieranheiberg/K-BOT.

Genome-scale metabolic modeling

Flux values for the metabolic map of *R. palustris* CGA009 were calculated using COBRApy with a genome-scale model based on iAN1128, with additional reactions to represent the heterologous PAD enzyme and transport reactions for the product of the engineered pathway, *p*-vinylphenol. Simulations were performed under photoheterotrophic conditions with *p*-CA as the sole carbon source. The code used to generate these flux values is available at https://github.com/carothersresearch/cSAGE.

Comparative genomic analysis

Alignments of the coumarate catabolic pathway genes between *R. palustris* CGA009 and P4 were performed using Mauve plugin in Geneious Prime v2026.0. The P4 genome is deposited in GenBank under Accession Number JBSYIN000000000. KEGG orthology (KO) analysis was performed using BLASTKoala for KO assignment.

Statistics and Reproducibility

All experiments were performed with at least three independent biological replicates, unless otherwise noted in the figure legends. For fluorescence and growth assays, values represent the mean of independent cultures with error bars indicating one standard deviation. For HPLC-based metabolite quantification, standard curves were prepared fresh for each experiment, and quantification was performed using at least three biological replicates. Integration efficiencies are reported as the mean proportion of colonies with correct integration, as determined by colony PCR. Plasmid sequences will be available upon publication.

Author contributions

†M.S.G. and C.K. contributed equally to this work. ⁺J.C. and A.R. contributed equally to this work. M.S.G., C.K., R.C., D.A. and J.E. conceived and designed the study. M.S.G., C.K., J.C., A.R., A.S, R.L.C., D.A.B., M.C., S.G., S.A., B.D., G.N.D, and D.H. performed experiments and analyzed the data. M.S.G., J.M.C., J.E., R.G.E, A.M.G, and A.B. supervised the project and guided data interpretation. A.B. and J.M.C. acquired funding. M.S.G., C.K., A.R., J.C., R.L.C., M.C., J.E., and J.M.C. wrote the manuscript with input from all authors.

Acknowledgements

We thank: Carrie Harwood and Yasuhiro Oda at the University of Washington for providing essential strains, protocols, and reagents that enabled this work; Huimin Zhao at the University of Illinois Urbana-Champaign for sharing *E. coli* WM6026; Eric Schaedig at The National Renewable Energy Laboratory and Carrie Eckhert at Oak Ridge National Laboratory who provided *Rubrivivax gelatinosus* CBS, as well as guidance and protocols for working with this strain. We thank Adam Guss at Oakridge National Laboratory for key bacterial strains and protocols. This research was supported by the DOE Office of Science, Office of Biological and Environmental Research (BER), grant no. DE-SC0023091. This report was prepared as an account of work sponsored by an agency of the United States Government. Neither the United States Government nor any agency thereof, nor any of their employees, makes any warranty, express or implied, or assumes any legal liability or responsibility for the accuracy, completeness, or usefulness of any information, apparatus, product, or process disclosed, or represents that its use would not infringe privately owned rights. Reference herein to any specific commercial product, process, or service by trade name, trademark, manufacturer, or otherwise does not necessarily constitute or imply its endorsement, recommendation, or favoring by the United States Government or any agency thereof. The views and opinions of the authors expressed herein do not necessarily state or reflect those of the United States Government or any agency thereof.

Figures and Tables

Table 1. Bacteria used in this study.

Organism	Classification	Origin	Primary bioproduction use cases
Rhodopseudomonas palustris CGA009	α-proteobacteria	Soil	Photosynthetic utilization of lignin breakdown products
Rhodopseudomonas palustris P4	α-proteobacteria	Anaerobic digester	Photosynthetic utilization of syngas
Rhodobacter sphaeroides ATH 2.4.1	α-proteobacteria	Freshwater	Isoprenoid biosynthesis and biohydrogen production
Rhodospirillum rubrum ATCC 11170	α-proteobacteria	Freshwater	Anaerobic syngas fermentation and CO/CO_2 assimilation
Rubrivivax gelatinosus CBS	β-proteobacteria	Soil	Photosynthetic fermentation of syngas and organic acids
Rhodococcus jostii RHA1	Actinobacteria	Soil	Lignin depolymerization and conversion of aromatic compounds
Pseudomonas sorgoleonovorans SO81	γ-proteobacteria	Rhizosphere	Plant-growth promotion and utilization of plant-derived carbon sources
Pseudomonas putida KT2440	γ-proteobacteria	Soil	Metabolic engineering platform for aromatic compound valorization

Table 2. cSAGE plasmid toolkit.

Plasmid	Intended use and key features
pRC414	Tn7-compatible landing pad integration; integrates poly-*attB* cassette at *attTn7*
pRC453	FLP recombinase; *sacB*
pCK1205	Integrase expression, Bxb1
pCK1206	Integrase expression, R4
pCK1207	Integrase expression, TG1
pSG010	Integrase expression, ΦC31 (marker curing / backbone excision)
pMG065	Payload integration, Bxb1 *attP*
pJC001	Payload integration, R4 *attP*
pBD0132	Payload integration, TG1 *attP*
pJC009	Payload integration with counterselection, poly-*attP* with *sacB*

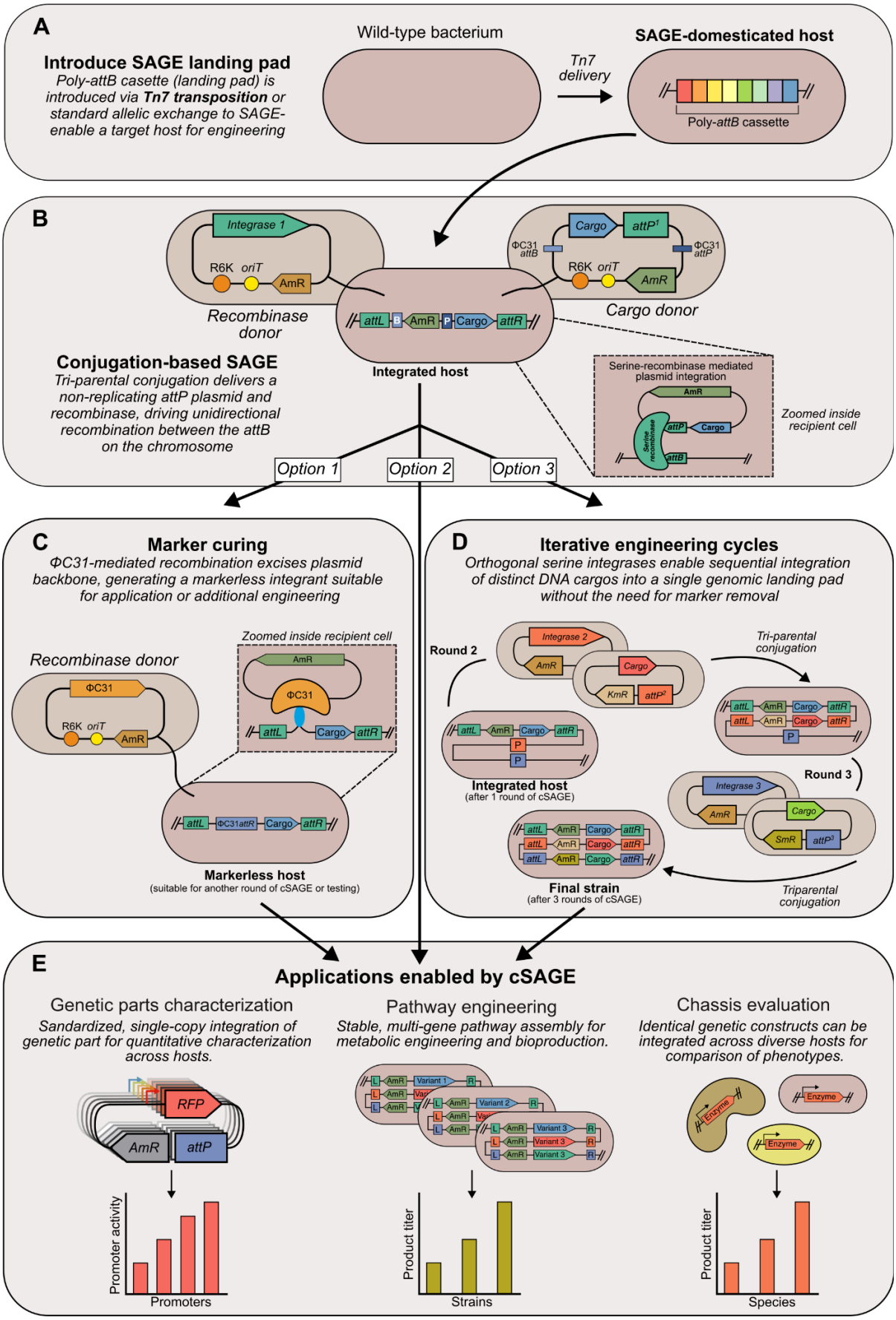

Figure 1. Workflow schematic of conjugation-compatible SAGE (cSAGE) integration and conjugation pipeline. (**A**) Establishing a SAGE-compatible host. A poly-*attB* landing pad containing multiple orthogonal recombinase target sites is introduced into the genome by Tn7 transposition or allelic exchange, generating a base strain compatible with serine recombinases-mediated engineering. (**B**) Conjugation-based genome integration. All SAGE plasmids were redesigned for compatibility with conjugative DNA transfer by incorporating an origin of transfer (oriT), adopting the Standard European Vector Architecture (SEVA) modular format, and using a *pir*-dependent R6K origin of replication that prevents replication in recipient hosts. The cSAGE workflow uses two non-replicating plasmids delivered by tri-parental conjugation: a cargo plasmid carrying an *attP* site and genetic payload, and a recombinase plasmid expressing a serine recombinase. Unidirectional recombination between chromosomal *attB* and plasmid *attP* sites drives stable integration of the payload. (**C**) Marker curing via ΦC31 integrase and counterselection. Following integration, markerless strains can be generated by a second conjugation step introducing a ΦC31 integrase-expressing helper plasmid, which excises the plasmid backbone and antibiotic marker through recombination between *att* sites. This results in a markerless genomic insertion suitable for subsequent engineering or testing. (**D**) Iterative integration cycles. Orthogonal serine recombinases (e.g., Bxb1, R4, TG1) enable sequential integration of multiple DNA cargos into a single genomic landing pad without requiring marker removal between rounds. Distinct antibiotic resistance markers and attachment sites allow independent selection of each integration, supporting multi-payload strain construction. (**E**) Applications enabled by cSAGE. cSAGE supports a wide range of genome engineering applications, including: (i) genetic part characterization via single-copy, standardized promoter–reporter fusions; (ii) pathway engineering through stable, multi-gene chromosomal assembly; and (iii) cross-host benchmarking across diverse bacterial species.

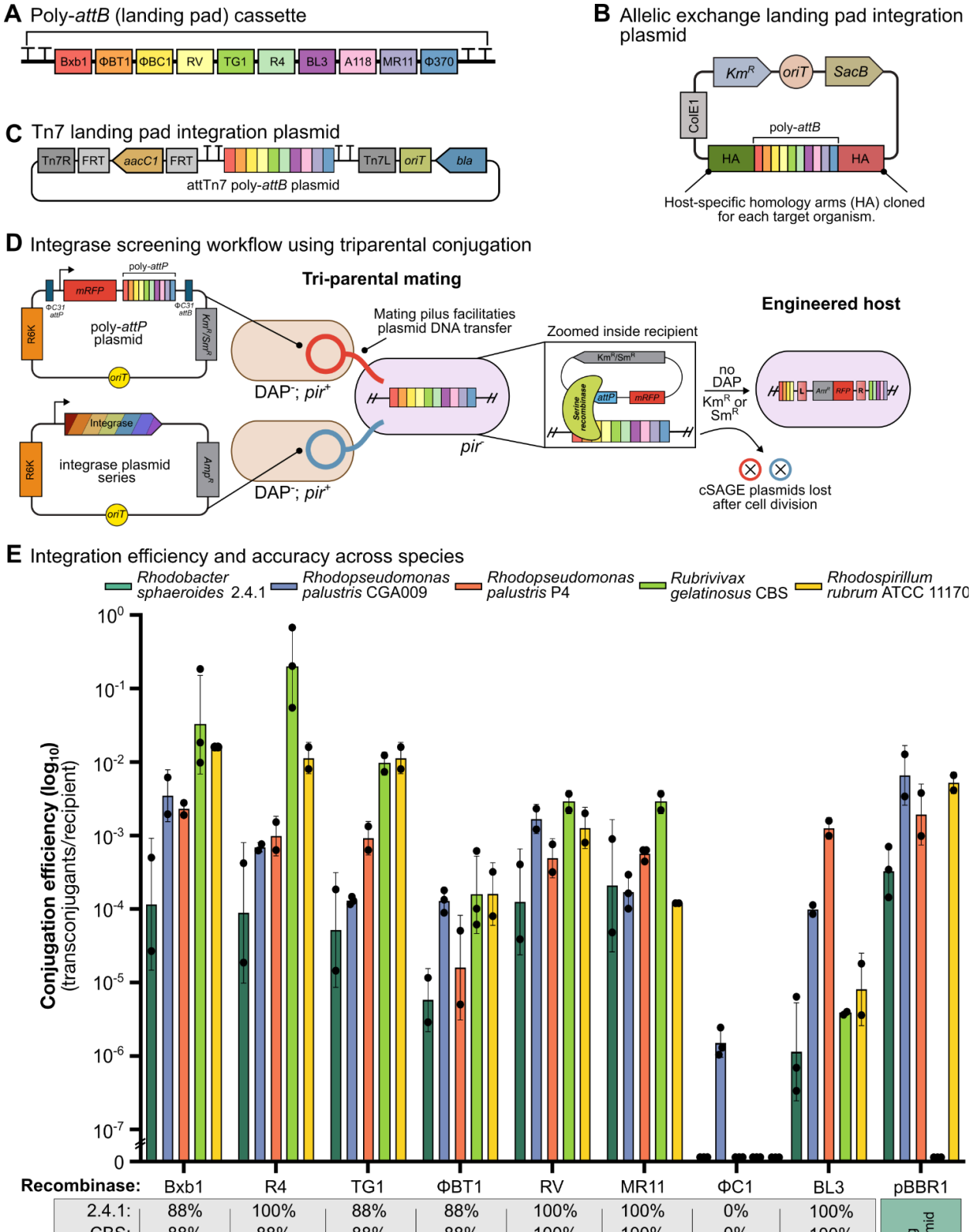

Recombinase:	Bxb1	R4	TG1	ΦBT1	RV	MR11	ΦC1	BL3	pBBR1
2.4.1:	88%	100%	88%	88%	100%	100%	0%	100%	Replicating control plasmid
CBS:	88%	88%	88%	88%	100%	100%	0%	100%	
CGA009:	100%	100%	100%	100%	100%	18%	36%	75%	
11170:	100%	100%	88%	100%	100%	50%	0%	100%	
P4:	83%	75%	58%	58%	100%	75%	0%	88%	

Figure 2. Conjugation-based SAGE (cSAGE) vector system, landing pad installation, and recombinase benchmarking across diverse hosts. (**A**) Design of the poly-*attB* landing pad. The genomic landing pad consists of ten orthogonal serine recombinase attachment sites (*attB*), each flanked by transcriptional terminators to prevent transcriptional readthrough and interference with neighboring loci. (**B**) Allelic exchange strategy. For species where Tn7 transposition was less efficient, the poly-attB cassette was integrated by allelic exchange using suicide vectors containing homology arms (HA) flanking the landing pad. Each vector includes an *oriT* for conjugative transfer, a *sacB* counterselection marker, and an antibiotic resistance cassette. (**C**) Tn7 transposon-based delivery system. A Tn7 delivery vector (pRC414) was constructed to integrate the poly-*attB* cassette into gram-negative bacterial genomes. The cassette is flanked by FRT recombination sites for optional marker removal and includes a gentamicin resistance marker (*aacC1*). (**D**) Recombinase screening via conjugation. Integration was tested using a tri-parental conjugation delivering two non-replicating plasmids: (i) a cargo plasmid containing a poly-attP array and a constitutively expressed mRFP reporter, and (ii) an integrase expression plasmid encoding one of eight serine recombinases (Bxb1, ΦBT1, ΦC1, RV, TG1, R4, BL3, MR11, A118, or Φ370). Recombination between the chromosomal attB site and plasmid-borne attP site results in stable integration of the mRFP cassette. Because all cSAGE plasmids use a pir-dependent R6K origin, they cannot replicate in recipient hosts and are lost after recombination. (**E**) Recombinases activity and fidelity across purple nonsulfur bacteria (PNSB). Conjugation efficiencies ($\log_{10}$ scale) are shown for eight recombinases tested in *Rhodobacter sphaeroides* 2.4.1, *Rubrivivax gelatinosus* CBS, *Rhodopseudomonas palustris* CGA009, *Rhodospirillum rubrum* 11170, and *R. palustris* P4. Each bar represents the average number of transconjugant colonies per recipient CFU ($n \geq 2$). A replicating control plasmid (pBBR1) was used to benchmark conjugation efficiency. The table below summarizes integration accuracy, defined as the proportion of colonies with correct on-target integrations confirmed by colony PCR ($n \geq 8$).

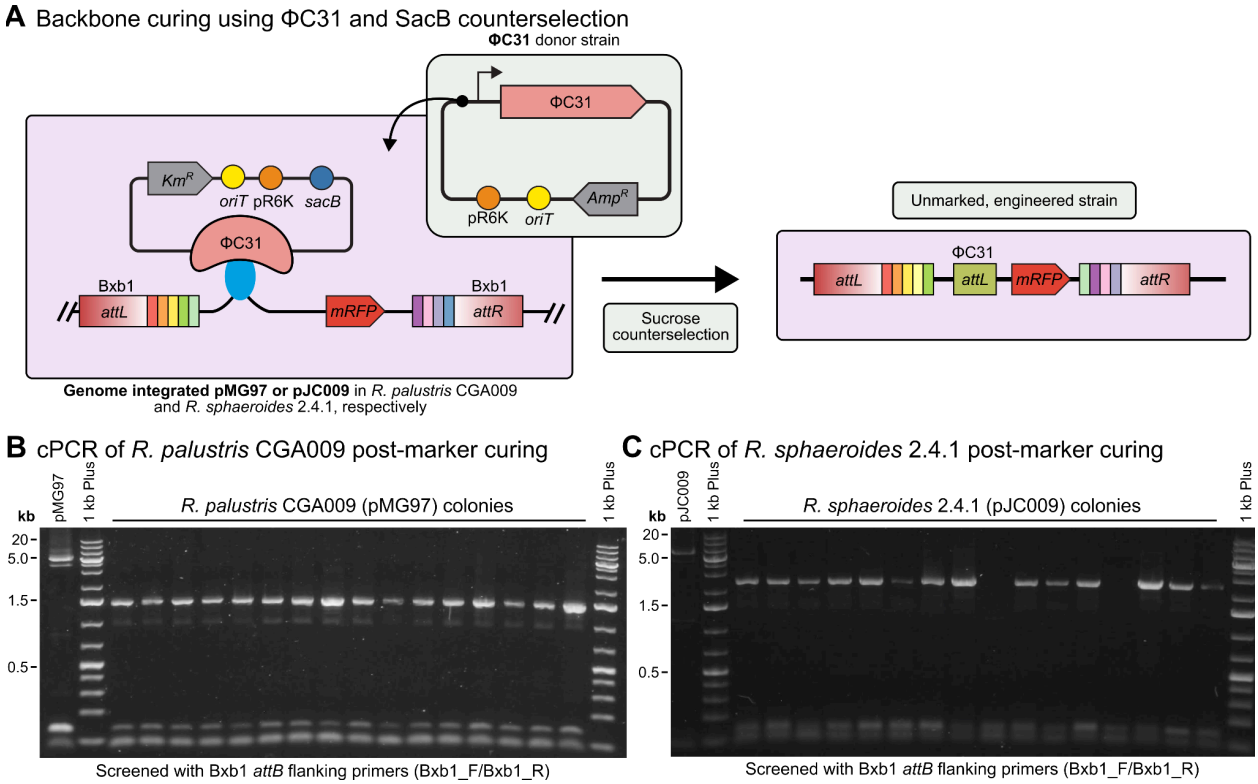

Figure 3. Marker recycling in cSAGE using ΦC31 integrase-mediated excision and sucrose counterselection. (**A**) ΦC31-based marker curing strategy. Genome-integrated poly-*attP* plasmids (pMG97 or pJC009) containing a constitutive *mRFP* reporter and a *sacB* counterselection cassette were flanked by ΦC31 *att* sites and delivered to *Rhodopseudomonas palustris* CGA009 or *Rhodobacter sphaeroides* 2.4.1 via cSAGE. A non-replicating ΦC31 integrase expression plasmid (pSG010) was subsequently introduced by conjugation to catalyze site-specific recombination between the ΦC31 *att* sites, excising the plasmid backbone and antibiotic resistance marker. The resulting markerless strain retains only the integrated cargo and minimal *attL*/*attR* scars. Following ΦC31-mediated recombination, sucrose counterselection was applied to remove residual cells retaining the *sacB* cassette/backbone. (**B-C**) Verification of marker excision. Colony PCR using primers flanking the Bxb1 *attB* integration site were used to distinguish between uncured (larger amplicon) and cured (smaller amplicon) strains. Gel electrophoresis of colony PCR products confirms precise ΦC31-mediated excision in both *R. palustris* CGA009 (left) and *R. sphaeroides* 2.4.1 (right). Expected band sizes: pMG97, 5125 bp (uncured) and 1461 bp (cured); pJC009, 6400 bp (uncured) and 2313 bp (cured).

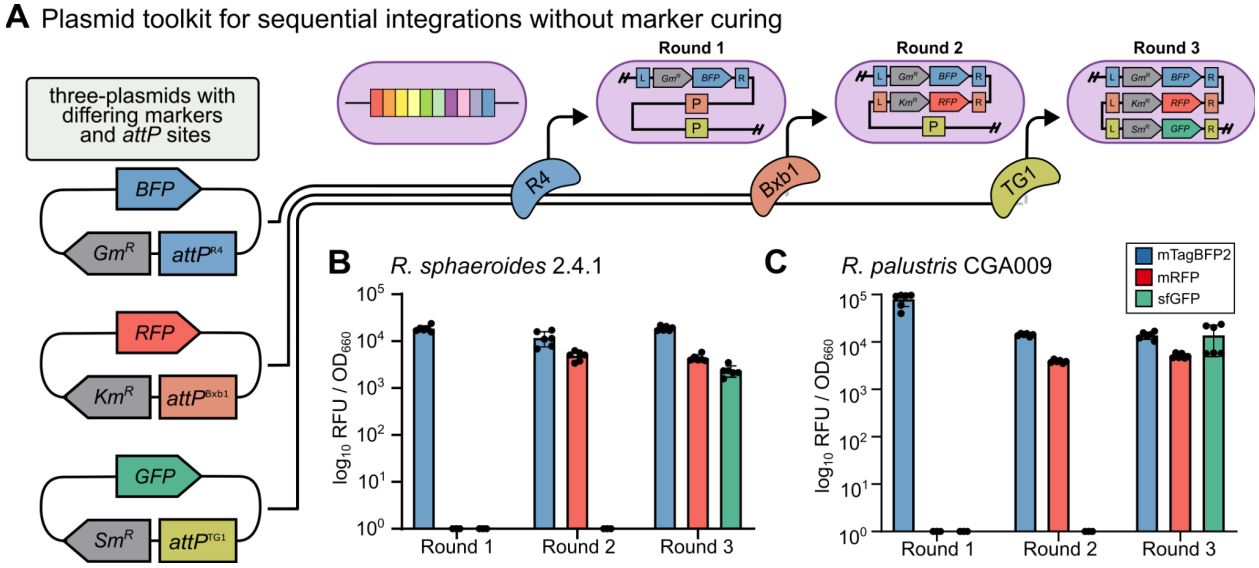

Figure 4. cSAGE toolkit for sequential multi-gene integrations. (A) Three-plasmid cSAGE integration system. A modular toolkit was developed for iterative genome engineering using orthogonal serine recombinases. Each plasmid carries a distinct fluorescent reporter (BFP, RFP, or GFP), a unique antibiotic resistance marker (Gm^R, Km^R, or Sm^R), and a specific *attP* site recognized by one of three serine recombinases (R4, Bxb1, or TG1, respectively). These features allow independent selection of each integration without the need for marker removal or counterselection between rounds. Integration proceeds through up to three rounds of conjugation, with each round introducing a new reporter cassette under the control of a constitutive promoter into a defined genomic landing pad. Orthogonal recombination sites ensure unidirectional and site-specific integration at each stage. (**B-C**) Quantitative reporter expression following sequential integrations. Fluorescence measurements for *Rhodobacter sphaeroides* 2.4.1 and *Rhodopseudomonas palustris* CGA009 after each integration cycle. Bars represent average normalized fluorescence (RFU/OD_{660}) of single colonies (n = 6) with error bars indicating standard deviation. Confirmed integrants from each round were propagated for subsequent integrations, and fluorescence from all reporters (new and previously integrated) was quantified to assess expression stability across successive engineering cycles.

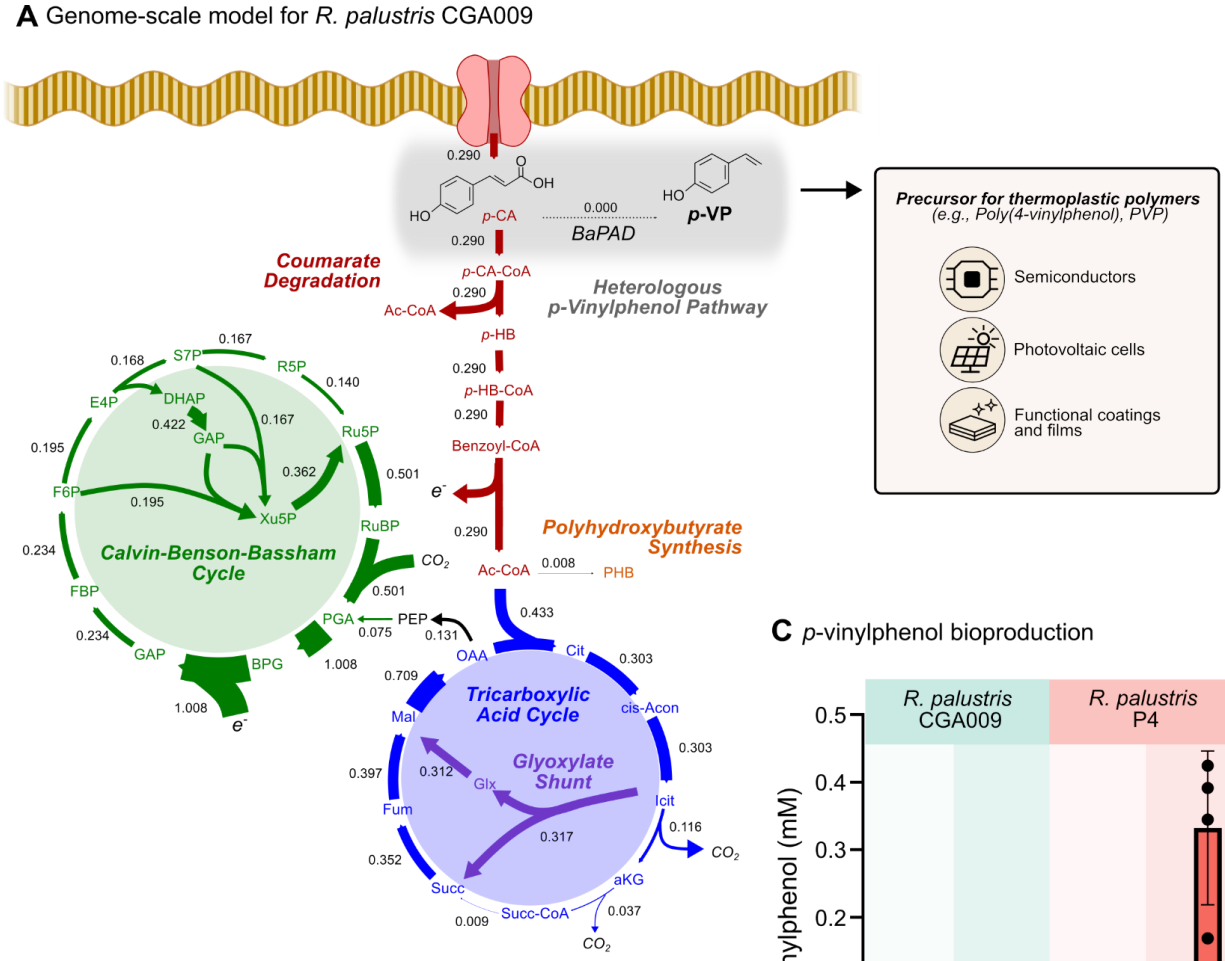

Figure 5. Photosynthetic bioproduction of *p*-vinylphenol in engineered PNSB. (**A**) Simulations of an iAN1128-based genome-scale model of engineered phenolic acid decarboxylase (PAD)-expressing *R. palustris* CGA009 grown photoheterotrophically on *p*-coumarate (*p*-CA). (**B**) Promoter activity across hosts. Fluorescence of integrated promoter constructs in *R. palustris* P4 and *R. palustris* CGA009. Data show relative fluorescence units (RFU) normalized to optical density (OD_{660}) for single colonies (n = 6; bars = mean ± s.d.). (**C**) *p*-vinylphenol production and *p*-CA consumption in *R. palustris* P4 and CGA009. Metabolite concentrations (*p*-VP and *p*-CA) were measured at inoculation (T_0) and after cultivation (T_f) for both wild-type (WT) and engineered (BaPAD) strains. *p*-VP is normalized to biomass at the time of sampling. Bar graphs are the mean ± s.d. of at least three biological replicates.

References

1. Zhang, C. *et al.* Economic and sustainable revolution to facilitate one-carbon biomanufacturing. *Nat. Commun.* **16**, 4896 (2025).
2. Eng, T. *et al.* Maximizing microbial bioproduction from sustainable carbon sources using iterative systems engineering. *Cell Rep.* **42**, 113087 (2023).
3. Ögmundarson, Ó., Sukumara, S., Herrgård, M. J. & Fantke, P. Combining Environmental and Economic Performance for Bioprocess Optimization. *Trends Biotechnol.* **38**, 1203–1214 (2020).
4. Garza Elizondo, A. M. *et al.* Building an expanded bio-based economy through synthetic biology. *Biotechnol. Adv.* **87**, 108775 (2026).
5. Zacharof, M.-P. & Lovitt, R. W. Complex Effluent Streams as a Potential Source of Volatile Fatty Acids. *Waste Biomass Valorization* **4**, 557–581 (2013).
6. Luo, K. *et al.* A critical review of volatile fatty acids produced from waste activated sludge: enhanced strategies and its applications. *Environ. Sci. Pollut. Res.* **26**, 13984–13998 (2019).
7. Wang, F. *et al.* Lignocellulosic biomass as sustainable feedstock and materials for power generation and energy storage. *J. Energy Chem.* **57**, 247–280 (2021).
8. Teixeira, L. V., Moutinho, L. F. & Romão-Dumaresq, A. S. Gas fermentation of C1 feedstocks: commercialization status and future prospects. *Biofuels Bioprod. Biorefining* **12**, 1103–1117 (2018).
9. Henstra, A. M., Sipma, J., Rinzema, A. & Stams, A. J. Microbiology of synthesis gas fermentation for biofuel production. *Curr. Opin. Biotechnol.* **18**, 200–206 (2007).
10. Romagnoli, S. & Tabita, F. R. Carbon dioxide metabolism and its regulation in nonsulfur purple photosynthetic bacteria. in *The purple phototrophic bacteria* 563–576 (Springer, 2009).
11. Morrison, H. M. & Bose, A. Purple non-sulfur bacteria for biotechnological applications. *J. Ind. Microbiol. Biotechnol.* **52**, kuae052 (2025).
12. Brown, B., Wilkins, M. & Saha, R. Rhodopseudomonas palustris: A biotechnology chassis. *Biotechnol. Adv.* **60**, 108001 (2022).
13. Orsi, E., Beekwilder, J., Eggink, G., Kengen, S. W. M. & Weusthuis, R. A. The transition of Rhodobacter sphaeroides into a microbial cell factory. *Biotechnol. Bioeng.* **118**, 531–541 (2021).
14. Tang, M. *et al.* The metabolic pathways of carbon assimilation and polyhydroxyalkanoate production by Rhodospirillum rubrum in response to different atmospheric fermentation. *PLOS ONE* **19**, e0306222 (2024).
15. Lu, H., Zhang, G., He, S., Zhao, R. & Zhu, D. Purple non-sulfur bacteria technology: a promising and potential approach for wastewater treatment and bioresources recovery. *World J. Microbiol. Biotechnol.* **37**, 161 (2021).
16. Revelles, O., Tarazona, N., García, J. L. & Prieto, M. A. Carbon roadmap from syngas to polyhydroxyalkanoates in Rhodospirillum rubrum. *Environ. Microbiol.* **18**, 708–720 (2016).
17. Kathol, M. *et al.* High enzyme promiscuity in lignin degradation mechanisms in Rhodopseudomonas palustris CGA009. *Appl. Environ. Microbiol.* **0**, e00573-25 (2025).
18. Bayon-Vicente, G. *et al.* Metabolic pathways to sustainability: review of purple non-sulfur bacteria potential in agri-food waste valorization. *Front. Bioeng. Biotechnol.* **13**, (2025).
19. Klamt, S., Grammel, H., Straube, R., Ghosh, R. & Gilles, E. D. Modeling the electron transport chain of purple non-sulfur bacteria. *Mol. Syst. Biol.* **4**, (2008).
20. Imam, S. *et al.* IRsp1095: A genome-scale reconstruction of the Rhodobacter sphaeroides metabolic network. *BMC Syst. Biol.* **5**, (2011).

21. Imam, S., Noguera, D. R. & Donohue, T. J. An Integrated Approach to Reconstructing Genome-Scale Transcriptional Regulatory Networks. *PLOS Comput. Biol.* **11**, e1004103 (2015).
22. Tec-Campos, D. *et al.* The genome-scale metabolic model for the purple non-sulfur bacterium Rhodopseudomonas palustris Bis A53 accurately predicts phenotypes under chemoheterotrophic, chemoautotrophic, photoheterotrophic, and photoautotrophic growth conditions. *PLOS Comput. Biol.* **19**, e1011371 (2023).
23. Cannon, W. R., King, E., Huening, K. A. & North, J. A. Redox poise in R. rubrum phototrophic growth drives large-scale changes in macromolecular pathways. *PLOS Comput. Biol.* **21**, e1013015 (2025).
24. Immethun, C. M., Kathol, M., Changa, T. & Saha, R. Synthetic Biology Tool Development Advances Predictable Gene Expression in the Metabolically Versatile Soil Bacterium Rhodopseudomonas palustris. *Front. Bioeng. Biotechnol.* **10**, (2022).
25. Freed, E. *et al.* Building a genome engineering toolbox in nonmodel prokaryotic microbes. *Biotechnol. Bioeng.* **115**, 2120–2138 (2018).
26. Yan, Q. & Fong, S. S. Challenges and Advances for Genetic Engineering of Non-model Bacteria and Uses in Consolidated Bioprocessing. *Front. Microbiol.* **8**, 2060 (2017).
27. Choi, K.-H. *et al.* A Tn7-based broad-range bacterial cloning and expression system. *Nat. Methods* **2**, 443–448 (2005).
28. Corts, A., Thomason, L. C., Costantino, N. & Court, D. L. Recombineering in Non-Model Bacteria. *Curr. Protoc.* **2**, e605 (2022).
29. Hwang, S., Joung, C., Kim, W., Palsson, B. & Cho, B.-K. Recent advances in non-model bacterial chassis construction. *Curr. Opin. Syst. Biol.* **36**, 100471 (2023).
30. Hall, A. N. *et al.* Tools for genetic engineering and gene expression control in Novosphingobium aromaticivorans and Rhodobacter sphaeroides. *Appl. Environ. Microbiol.* **0**, e00348-24 (2024).
31. Mougiakos, I. *et al.* Efficient Cas9-based genome editing of Rhodobacter sphaeroides for metabolic engineering. *Microb. Cell Factories* **18**, (2019).
32. Hwang, S., Joung, C., Kim, W., Palsson, B. & Cho, B.-K. Recent advances in non-model bacterial chassis construction. *Curr. Opin. Syst. Biol.* **36**, 100471 (2023).
33. Gilbert, C. *et al.* A scalable framework for high-throughput identification of functional origins of replication in non-model bacteria. 2023.05.19.541510 Preprint at https://doi.org/10.1101/2023.05.19.541510 (2023).
34. Vento, J. M., Crook, N. & Beisel, C. L. Barriers to genome editing with CRISPR in bacteria. *J. Ind. Microbiol. Biotechnol.* **46**, 1327–1341 (2019).
35. Thomas, C. M. & Nielsen, K. M. Mechanisms of, and Barriers to, Horizontal Gene Transfer between Bacteria. *Nat. Rev. Microbiol.* **3**, 711–721 (2005).
36. LeBlanc, N. & Charles, T. C. Bacterial genome reductions: Tools, applications, and challenges. *Front. Genome Ed.* **4**, (2022).
37. Rohmat, R. K. W. *et al.* Emerging trends in genome integration tools for precision engineering of diverse bacterial species. *Synth. Biol.* **10**, ysaf019 (2025).
38. Rubin, B. E. *et al.* Species- and site-specific genome editing in complex bacterial communities. *Nat. Microbiol.* **7**, 34–47 (2022).
39. Riley, L. A. & Guss, A. M. Approaches to genetic tool development for rapid domestication of non-model microorganisms. *Biotechnol. Biofuels* **14**, 30 (2021).
40. Liu, Z., Liang, Y., Ang, E. L. & Zhao, H. A New Era of Genome Integration—Simply Cut and Paste! *ACS Synth. Biol.* **6**, 601–609 (2017).
41. Lu, L. *et al.* CRISPR-based metabolic engineering in non-model microorganisms. *Curr. Opin. Biotechnol.* **75**, 102698 (2022).

42. Peters, J. M. *et al.* Enabling genetic analysis of diverse bacteria with Mobile-CRISPRi. *Nat. Microbiol.* **4**, 244–250 (2019).
43. Ashok, N. *et al.* Thermophilic site-specific recombination system for rapid insertion of heterologous DNA into the Clostridium thermocellum chromosome. *J. Ind. Microbiol. Biotechnol.* **52**, kuaf023 (2024).
44. Elmore, J. R. *et al. High-Throughput Genetic Engineering of Nonmodel and Undomesticated Bacteria via Iterative Site-Specific Genome Integration*. https://www.science.org (2023).
45. Li, L. *et al.* aMSGE: advanced multiplex site-specific genome engineering with orthogonal modular recombinases in actinomycetes. *Metab. Eng.* **52**, 153–167 (2019).
46. Snoeck, N. *et al.* Serine integrase recombinational engineering (SIRE): A versatile toolbox for genome editing. *Biotechnol. Bioeng.* **116**, 364–374 (2019).
47. Elmore, J. R., Furches, A., Wolff, G. N., Gorday, K. & Guss, A. M. Development of a high efficiency integration system and promoter library for rapid modification of *Pseudomonas putida* KT2440. *Metab. Eng. Commun.* **5**, 1–8 (2017).
48. Merrick, C. A., Zhao, J. & Rosser, S. J. Serine Integrases: Advancing Synthetic Biology. *ACS Synth. Biol.* **7**, 299–310 (2018).
49. De La Cruz, F., Frost, L. S., Meyer, R. J. & Zechner, E. L. Conjugative DNA metabolism in Gram-negative bacteria. *FEMS Microbiol. Rev.* **34**, 18–40 (2010).
50. Grohmann, E., Muth, G. & Espinosa, M. Conjugative Plasmid Transfer in Gram-Positive Bacteria. *Microbiol. Mol. Biol. Rev.* **67**, 277–301 (2003).
51. Davison, J. Genetic Exchange between Bacteria in the Environment. *Plasmid* **42**, 73–91 (1999).
52. Samuel, B., Mittelman, K., Croitoru, S. Y., Ben Haim, M. & Burstein, D. Diverse anti-defence systems are encoded in the leading region of plasmids. *Nature* **635**, 186–192 (2024).
53. Dimitriu, T., Szczelkun, M. D. & Westra, E. R. Various plasmid strategies limit the effect of bacterial restriction–modification systems against conjugation. *Nucleic Acids Res.* **52**, 12976–12986 (2024).
54. Purdy, D. *et al.* Conjugative transfer of clostridial shuttle vectors from Escherichia coli to Clostridium difficile through circumvention of the restriction barrier. *Mol. Microbiol.* **46**, 439–452 (2002).
55. Wang, G. *et al.* CRAGE enables rapid activation of biosynthetic gene clusters in undomesticated bacteria. *Nat. Microbiol.* **4**, 2498–2510 (2019).
56. Zhao, Z., Cheng, J.-F. & Yoshikuni, Y. Chromosomal integration of complex DNA constructs using CRAGE and CRAGE-Duet systems. *STAR Protoc.* **3**, 101546 (2022).
57. Elston, K. M. *et al.* The Pathfinder plasmid toolkit for genetically engineering newly isolated bacteria enables the study of Drosophila-colonizing Orbaceae. *ISME Commun.* **3**, 49 (2023).
58. Geddes, B. A., Mendoza-Suárez, M. A. & Poole, P. S. A Bacterial Expression Vector Archive (BEVA) for Flexible Modular Assembly of Golden Gate-Compatible Vectors. *Front. Microbiol.* **9**, (2019).
59. Schuster, L. A. & Reisch, C. R. A plasmid toolbox for controlled gene expression across the Proteobacteria. *Nucleic Acids Res.* **49**, 7189–7202 (2021).
60. Christi, K., Hudson, J. & Egan, S. Current approaches to genetic modification of marine bacteria and considerations for improved transformation efficiency. *Microbiol. Res.* **284**, 127729 (2024).
61. Samperio, S. *et al.* Conjugative DNA Transfer From E. coli to Transformation-Resistant Lactobacilli. *Front. Microbiol.* **12**, (2021).

62. Brumwell, S. L., Van Belois, K. D., Giguere, D. J., Edgell, D. R. & Karas, B. J. Conjugation-Based Genome Engineering in Deinococcus radiodurans. *ACS Synth. Biol.* **11**, 1068–1076 (2022).
63. Liu, X. *et al.* Construction of conjugative gene transfer system between E. coli and moderately thermophilic, extremely acidophilic Acidithiobacillus caldus MTH-04. *J. Microbiol. Biotechnol.* **17**, 162–167 (2007).
64. Tominaga, Y., Ohshiro, T. & Suzuki, H. Conjugative plasmid transfer from Escherichia coli is a versatile approach for genetic transformation of thermophilic Bacillus and Geobacillus species. *Extremophiles* **20**, 375–381 (2016).
65. Gelsinger, D. R. *et al.* Metagenomic editing of commensal bacteria in vivo using CRISPR-associated transposases. *Science* **390**, eadx7604 (2025).
66. Ronda, C. *et al.* Precise virulence inactivation using a CRISPR-associated transposase for combating Enterobacteriaceae gut pathogens. *Nat. Biomed. Eng.* **9**, 2017–2027 (2025).
67. Martínez-García, E. *et al.* SEVA 4.0: an update of the Standard European Vector Architecture database for advanced analysis and programming of bacterial phenotypes. *Nucleic Acids Res.* **51**, D1558–D1567 (2023).
68. Silva-Rocha, R. *et al.* The Standard European Vector Architecture (SEVA): a coherent platform for the analysis and deployment of complex prokaryotic phenotypes. *Nucleic Acids Res.* **41**, D666–D675 (2013).
69. Ares-Arroyo, M., Coluzzi, C. & Rocha, E. P. C. Origins of transfer establish networks of functional dependencies for plasmid transfer by conjugation. *Nucleic Acids Res.* **51**, 3001–3016 (2023).
70. Rakowski, S. A. & Filutowicz, M. Plasmid R6K replication control. *Plasmid* **69**, 231–242 (2013).
71. Metcalf, W. W., Jiang, W. & Wanner, B. L. Use of the *rep* technique for allele replacement to construct new *Escherichia coli* hosts for maintenance of R6Kλ origin plasmids at different copy numbers. *Gene* **138**, 1–7 (1994).
72. Kittleson, J. T., Cheung, S. & Anderson, Jc. Rapid optimization of gene dosage in E. coli using DIAL strains. *J. Biol. Eng.* **5**, 10 (2011).
73. Jung, G. Y., Jung, H. O., Kim, J. R., Ahn, Y. & Park, S. Isolation and characterization of Rhodopseudomonas palustris P4 which utilizes CO with the production of H2. *Biotechnol. Lett.* **21**, 525–529 (1999).
74. Kontur, W. S. *et al.* Revised sequence and annotation of the Rhodobacter sphaeroides 2.4.1 genome. *J. Bacteriol.* **194**, 7016–7017 (2012).
75. Munk, A. C. *et al.* Complete genome sequence of Rhodospirillum rubrum type strain (S1T). *Stand. Genomic Sci.* **4**, 293–302 (2011).
76. Hu, P. *et al.* Draft Genome Sequence of Rubrivivax gelatinosus CBS. *J. Bacteriol.* **194**, 3262 (2012).
77. Jun, D., Saer, R. G., Madden, J. D. & Beatty, J. T. Use of new strains of Rhodobacter sphaeroides and a modified simple culture medium to increase yield and facilitate purification of the reaction centre. *Photosynth. Res.* **120**, 197–205 (2014).
78. Lee, Y. R. *et al.* Optimization of Electroporation Conditions for Introducing Heterologous DNA into Rhodobacter sphaeroides. **34**, 1–6 (2024).
79. Kovach, M. E. *et al. Four New Derivatives of the Broad-Host-Range Cloning Vector pBBR1MCS, Carrying Different Antibiotic-Resistance Cassettes*. *Gene* vol. 166 175–176 (1995).
80. Loeschcke, A. & Thies, S. Pseudomonas putida—a versatile host for the production of natural products. *Appl. Microbiol. Biotechnol.* **99**, 6197–6214 (2015).

81. Nikel, P. I., Chavarría, M., Danchin, A. & de Lorenzo, V. From dirt to industrial applications: *Pseudomonas putida* as a Synthetic Biology *chassis* for hosting harsh biochemical reactions. *Curr. Opin. Chem. Biol.* **34**, 20–29 (2016).
82. Sorgoleone degradation by sorghum-associated bacteria; an opportunity for enforcing plant growth promotion | bioRxiv. https://www.biorxiv.org/content/10.1101/2023.05.26.542311v1.abstract.
83. Cappelletti, M. *et al.* Biotechnology of Rhodococcus for the production of valuable compounds. *Appl. Microbiol. Biotechnol.* **104**, 8567–8594 (2020).
84. Larkin, M. J., Kulakov, L. A. & Allen, C. C. Biodegradation and Rhodococcus – masters of catabolic versatility. *Curr. Opin. Biotechnol.* **16**, 282–290 (2005).
85. Lammens, E.-M., Nikel, P. I. & Lavigne, R. Exploring the synthetic biology potential of bacteriophages for engineering non-model bacteria. *Nat. Commun.* **11**, 5294 (2020).
86. Martinez, J. L. The role of natural environments in the evolution of resistance traits in pathogenic bacteria. *Proc. R. Soc. B Biol. Sci.* **276**, 2521–2530 (2009).
87. Reyrat, J.-M., Pelicic, V., Gicquel, B. & Rappuoli, R. Counterselectable Markers: Untapped Tools for Bacterial Genetics and Pathogenesis. *Infect. Immun.* **66**, 4011–4017 (1998).
88. Hernandez-Maldonado, J. *et al.* The genetic basis of anoxygenic photosynthetic arsenite oxidation. *Environ. Microbiol.* **19**, 130–141 (2017).
89. Raschdorf, O., Plitzko, J. M., Schüler, D. & Müller, F. D. A Tailored galK Counterselection System for Efficient Markerless Gene Deletion and Chromosomal Tagging in Magnetospirillum gryphiswaldense. *Appl. Environ. Microbiol.* **80**, 4323–4330 (2014).
90. Ledermann, R., Strebel, S., Kampik, C. & Fischer, H.-M. Versatile Vectors for Efficient Mutagenesis of Bradyrhizobium diazoefficiens and Other Alphaproteobacteria. *Appl. Environ. Microbiol.* **82**, 2791–2799 (2016).
91. Silo-Suh, L. A., Elmore, B., Ohman, D. E. & Suh, S.-J. Isolation, characterization, and utilization of a temperature-sensitive allele of a *Pseudomonas* replicon. *J. Microbiol. Methods* **78**, 319–324 (2009).
92. Pan, C. *et al.* Characterization of Anaerobic Catabolism of *p*-Coumarate in *Rhodopseudomonas palustris* by Integrating Transcriptomics and Quantitative Proteomics*. *Mol. Cell. Proteomics* **7**, 938–948 (2008).
93. Austin, S. *et al.* Metabolism of Multiple Aromatic Compounds in Corn Stover Hydrolysate by Rhodopseudomonas palustris. *Environ. Sci. Technol.* **49**, 8914–8922 (2015).
94. Harwood, C. S. & Gibson, J. Anaerobic and aerobic metabolism of diverse aromatic compounds by the photosynthetic bacterium Rhodopseudomonas palustris. *Appl. Environ. Microbiol.* **54**, 712–717 (1988).
95. Harwood, C. S. & Gibson, J. Uptake of benzoate by Rhodopseudomonas palustris grown anaerobically in light. *J. Bacteriol.* **165**, 504–509 (1986).
96. Doki, M. M. *et al.* Recovery of purple non-sulfur bacteria-mediated single-cell protein from domestic wastewater in two-stage treatment using high rate digester and raceway pond. *Bioresour. Technol.* **413**, 131467 (2024).
97. Hädicke, O., Grammel, H. & Klamt, S. Metabolic network modeling of redox balancing and biohydrogen production in purple nonsulfur bacteria. *BMC Syst. Biol.* **5**, (2011).
98. Navid, A., Jiao, Y., Wong, S. E. & Pett-Ridge, J. System-level analysis of metabolic trade-offs during anaerobic photoheterotrophic growth in Rhodopseudomonas palustris. *BMC Bioinformatics* **20**, 233 (2019).
99. Fang, X., Lloyd, C. J. & Palsson, B. O. Reconstructing organisms in silico: genome-scale models and their emerging applications. *Nat. Rev. Microbiol.* **18**, 731–743 (2020).
100. Hirakawa, H., Schaefer, A. L., Greenberg, E. P. & Harwood, C. S. Anaerobic p-Coumarate Degradation by Rhodopseudomonas palustris and Identification of CouR, a MarR

Repressor Protein That Binds p-Coumaroyl Coenzyme A. *J. Bacteriol.* **194**, 1960–1967 (2012).
101. Liu, R.-Y., Liu, Z.-H., Li, B.-Z. & Yuan, Y.-J. Biotransformation of lignin into 4-vinylphenol derivatives toward lignin valorization. *Green Chem.* **26**, 1770–1789 (2024).
102. Uppalapati, S., Kong, N., Norberg, O., Ramström, O. & Yan, M. Ionization of covalent immobilized poly(4-vinylphenol) monolayers measured by ellipsometry, QCM and SPR. *Appl. Surf. Sci.* **343**, 166–171 (2015).
103. Peshkova, S. & Li, K. Investigation of Poly(4-Vinylphenol) As a Wood Adhesive. *Wood Fiber Sci.* 41–48 (2003).
104. Zhang, G., Kim, C. & Choi, W. Poly(4-vinylphenol) as a new stable and metal-free sensitizer of titania for visible light photocatalysis through ligand-to-metal charge transfer process. *Catal. Today* **281**, 109–116 (2017).
105. Fontana, J. *et al.* Effective CRISPRa-mediated control of gene expression in bacteria must overcome strict target site requirements. *Nat. Commun.* **11**, (2020).
106. Kiattisewee, C. *et al.* Portable bacterial CRISPR transcriptional activation enables metabolic engineering in Pseudomonas putida. *Metab. Eng.* **66**, 283–295 (2021).
107. Singh, S., Ghosh, P. & Hatfull, G. F. Attachment site selection and identity in Bxb1 serine integrase-mediated site-specific recombination. *PLoS Genet.* **9**, e1003490 (2013).
108. Xu, Z. *et al.* Accuracy and efficiency define Bxb1 integrase as the best of fifteen candidate serine recombinases for the integration of DNA into the human genome. *BMC Biotechnol.* **13**, 87 (2013).
109. Bakalar, M. H. *et al.* Large Serine Integrase Off-Target Discovery with Deep Learning for Genome Wide Prediction. 2024.10.10.617699 Preprint at https://doi.org/10.1101/2024.10.10.617699 (2024).
110. Hazelbaker, D. Z. *et al.* Large Serine Integrase Off-target Discovery and Validation for Therapeutic Genome Editing. 2024.08.23.609471 Preprint at https://doi.org/10.1101/2024.08.23.609471 (2024).
111. Lei, X., Wang, L., Zhao, G. & Ding, X. Site-specificity of serine integrase demonstrated by the attB sequence preference of ϕBT1 integrase. *FEBS Lett.* **592**, 1389–1399 (2018).
112. Durrant, M. G. *et al.* Systematic discovery of recombinases for efficient integration of large DNA sequences into the human genome. *Nat. Biotechnol.* **41**, 488–499 (2023).
113. Burbano, D. A. *et al.* CRISPR Tools for Engineering Prokaryotic Systems: Recent Advances and New Applications. *Annu. Rev. Chem. Biomol. Eng.* **15**, 389–430 (2024).
114. Elmore, J. R. *et al.* Reinforced CRISPR interference enables reliable multiplex gene repression in phylogenetically distant bacteria. 2025.04.14.648646 Preprint at https://doi.org/10.1101/2025.04.14.648646 (2025).
115. Huenemann, J. D. *et al.* Combinatorial pathway engineering using multiplex Serine recombinase-Assisted Genome Engineering (mSAGE). 2025.07.11.664204 Preprint at https://doi.org/10.1101/2025.07.11.664204 (2025).
116. Fossen, E. M. V. *et al.* Efficient genetic code expansion tools enable in vivo study of lysine acetylation in non-model bacteria. 2025.04.14.648644 Preprint at https://doi.org/10.1101/2025.04.14.648644 (2025).
117. Blodgett, J. A. V. *et al.* Unusual transformations in the biosynthesis of the antibiotic phosphinothricin tripeptide. *Nat. Chem. Biol.* **3**, 480–485 (2007).
118. Fenster, J. A. *et al.* Dynamic and single cell characterization of a CRISPR-interference toolset in *Pseudomonas putida* KT2440 for β-ketoadipate production from *p*-coumarate. *Metab. Eng. Commun.* **15**, e00204 (2022).
119. Deutzmann, J. S. *et al.* Low-Cost Clamp-On Photometers (ClampOD) and Tube Photometers (TubeOD) for Online Cell Density Determination. *Front. Microbiol.* **12**, (2022).